We are IntechOpen,
the world's leading publisher of Open Access books
Built by scientists, for scientists

6,100
Open access books available

149,000
International authors and editors

185M
Downloads

154
Countries delivered to

Our authors are among the

TOP 1%
most cited scientists

12.2%
Contributors from top 500 universities

WEB OF SCIENCE™

Selection of our books indexed in the Book Citation Index
in Web of Science™ Core Collection (BKCI)

Interested in publishing with us?
Contact book.department@intechopen.com

Numbers displayed above are based on latest data collected.
For more information visit www.intechopen.com

Chapter

Simulation Study of Microwave Heating of Hematite and Coal Mixture

*Prasenjit Singha, Sunil Yadav, Soumya Ranjan Mohanty,
Abhishek Tiwari and Ajay Kumar Shukla*

Abstract

Temperature distribution in hematite ore mixed with 7.5% coal was predicted by solving a 1-D heat conduction equation using an implicit finite difference approach. In this work, a square slab of 20 cm x 20 cm was considered, which assumed the coal to be uniformly mixed with hematite ore. MATLAB 2018a software was used to solve the equations. Heat transfer effects in this one dimensional slab having convective and the radiative boundary conditions are also considered in this study. Temperature distribution is obtained inside the hematite slab by considering microwave heating time, thermal conductivity, heat capacity, carbon percentage, sample dimensions, and many other factors, such as penetration depth, permittivity, and permeability of coal and hematite ore mixtures. The resulting temperature profile used as a guiding tool for optimizing the microwave-assisted carbothermal reduction process of hematite slab which was extended to other dimensions as well, viz., 1 cm x 1 cm, 5 cm x 5 cm, 10 cm x 10 cm, and 20 cm x 20 cm. The model predictions are in good agreement with experimental results.

Keywords: Hematite ore, coal, microwave processing, heat transfer, implicit method, temperature distribution

1. Introduction

Current iron and steel-making industries are experiencing challenges, such as low-grade ore (<35% iron), poor sintering performance, and CO_2 gas emissions. FASTMET, ITmk3, and Hi-QIP processes can be adopted to increase the iron concentration of low-grade ores. For such processes, a mixture of powdery iron ore and carbonaceous material is used as raw materials, whereas the conductive heat flow from the surface to the interior of materials is the rate-controlling step, resulting in decreased productivity. The demand for microwave heating is escalating day to day in iron-making industries owing to its faster heating rate, volumetric heat generation for specific materials, energy savings, and less processing time [1–7]. Hematite can be converted to magnetite for iron ore beneficiation purposes. It can be achieved by heating the hematite. There are two ways of heating: one, conventional heating, and

second, microwave heating. In any conventional heating processes, along with hematite, other impurity oxides will be heated, which is not beneficial. This unnecessary heating can be bypassed by adopting microwave heating. In microwave heating, high efficiency in heating can be achieved because not all impurity oxides are heated, such as SiO_2 and Al_2O_3 [8]. Hayashi et al. [7] experimentally generated temperature versus time profile and predicted the effect of graphite content on the temperature characteristic of a mixture of hematite and graphite powders. Standish and Huang [9] investigated the reduction behaviors of hematite fines by mixing carbon and suggested microwave reduction in a non-isothermal process, and the temperature had a significant impact on the reduction of hematite fines. Agrawal and Dhawan [10] evaluated the reduction behavior of low iron hematite ore containing coke and charcoal and reported coke to be a better reductant than charcoal. Mishra and Roy [11] introduced carbon content that has an important effect on the reduction efficiency of the iron ore–coal composite pellet. They [11] obtained a 70% degree of reduction at 1250°C for 20 minutes when the C to Fe_2O_3 molar ratio is three. Zhulin et al. [12] presented the effect of carbon content on the reduction efficiency of iron ore–coal composite pellets at 1200°C for 15 minutes and predicted higher carbon-containing pellets reduced faster than lower carbon pellets. Mourao et al. [13] have demonstrated the reduction rate and maximum temperature of process depending upon the fraction of carbonaceous material. The author found that if the fraction of carbonaceous material increases in the mixture of hematite ore and carbonaceous material, the maximum temperature increases in the process, which increases the reduction reaction rate of hematite ore. Mishra et al. [14] have developed a thermal profile considering powder size, emissivity, and susceptibility using microwave heating, and reported model predictions are in good agreement with experiment results. The previous studies [7–14] experimentally demonstrated coke or coal to have a significant effect on temperature and reduction rate of hematite ore. However, their work lacks temperature distribution during the process. Shukla et al. [15] simulated temperature distribution in 2D cylinders of varying radii and physical properties using an explicit infinite method and found that the efficacy of temperature distribution in cylinders depends on the sample size and its thermal conductivity. They considered constant thermal conductivity and heat capacity throughout the process. Peng et al. [16] have demonstrated the heat transfer numerically during microwave heating of magnetite 1D slab. They solved the heat equation using an explicit infinite method based on fewer dimensions. Peng et al. [17] predicted the dielectric and magnetic behavior of the nonstoichiometric ferrous oxide at 823 K and 1373 K, respectively, and evaluated the temperature dependence of the microwave absorption capability of the ferrous oxide by considering the phase transformation during heating. Leo et al. [18] have shown effective permittivity of soils using Lichtenecker's mixing model. Although microwaves have superiority in materials heating, a major drawback known as nonuniform temperature distribution inside materials has also been observed [5, 6]. To address this problem, accurate temperature determination inside the materials under microwave irradiation is necessary. For last 30 years, microwave heating has been utilized extensively in the food processing industry. Most of those works considered heat diffusion and or convection to predict the temperature distribution in the material.

Although a lot of work has been done on microwave heating, the present study investigates the heat transfer process in microwave heating to predict the temperature distribution inside a 1D hematite slab using an implicit finite-difference approach by considering heat diffusion convection and radiation effects. The objective of the

current study is to design and produce a well-defined heating profile in a 1D rectangular slab of hematite ores using microwave heating routes. The resulting temperature profile can be used as a guiding tool to optimize the carbothermal reduction process of hematite in industry, where we studied on large slab (20 cm x 20 cm) as well as laboratory approach small slab (1 cm x 1 cm).

2. Mathematical formulation

The microwave heating process is modeled using a 1D heat transfer equation given below.

$$\frac{\partial T}{\partial t} = \frac{1}{\rho c_p} \frac{\partial k}{\partial x} \frac{\partial T}{\partial x} + \frac{k}{\rho c_p} \frac{\delta T^2}{\delta x^2} + \frac{P(x)}{\rho c_p} \tag{1}$$

$$P(x) = \frac{P_0}{D_p} \times \left(\exp{(X - x)}/D_p \right) \tag{2}$$

$$D_p \, (\text{depth of penetration}) = \frac{\lambda_0}{2 * \pi \sqrt{(2 * \mu_r')}} * \left\{ \left[1 + \left(\frac{\varepsilon_r''}{\varepsilon_r'} \right)^2 \right]^{1/2} - 1 \right\}^{-\frac{1}{2}} \tag{3}$$

Eq. (1) was discretized to study the heat distribution in each node with respect to time. The slab was discretized into 50×50 nodes using the equations given below.

$$\frac{\partial T}{\partial x} = \frac{T_{i+1,}^{n+1} - T_{i-1}^{n+1}}{2\delta x} \tag{4}$$

$$\frac{\partial k}{\partial x} = \frac{k_{i+1}^{n+1} - k_{i-1}^{n+1}}{2\delta k} \tag{5}$$

$$\frac{\delta T^2}{\delta x^2} \frac{T_{i+1}^{n+1} - 2\,T_i^{n+1} + T_{i-1}^{n+1}}{\delta x^2} \tag{6}$$

The schematic representation of a square slab with node points is shown in **Figure 1**. Here, i represents the horizontal domain, and i+1 and i−1 represent forward and backward nodes, respectively. Where i, varying from 1 to M, $i = 1$ represents the left boundary, and $i = M$ represents the right boundary. The time-domain [0, t] was divided into n segments, each of duration $\delta t = t/n$.

The implicit finite difference approximation method was used in this study, where the governing equations were discretized (**Figure 1**) into different domains in the form of node points.

Model assumptions are as follows

1. Heat source is uniformly distributed.

2. No change in properties after mixing ore and coal

3. Ash and volatile matter does not affect the loss factor and dielectric constant of the mixture (**Figure 2**)
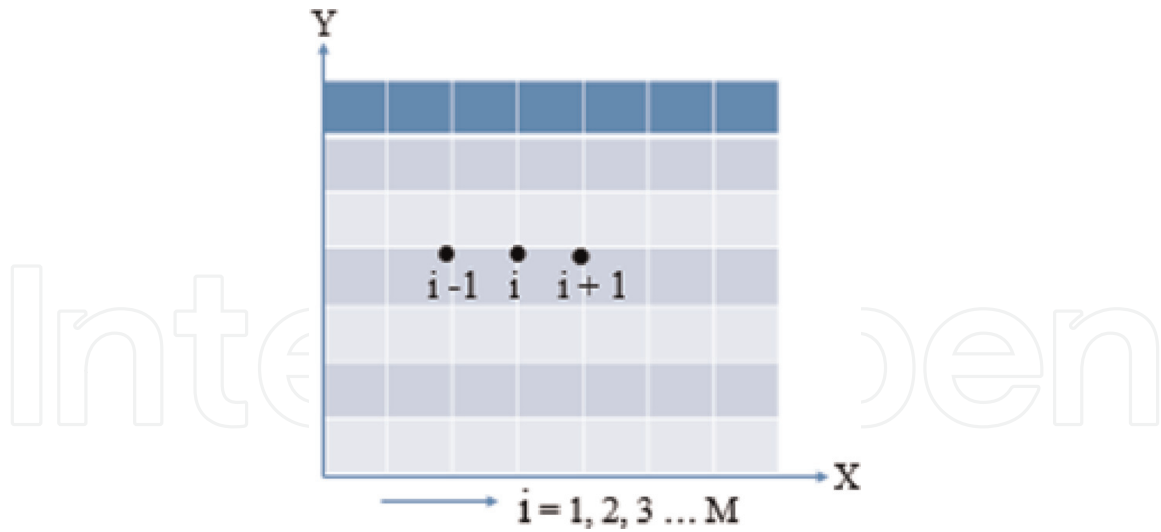
Figure 1.
Schematic representation of a square slab with node points i representing the horizontal domain, and i+1 and i−1 represent forward and backward nodes, respectively.

2.1 Modeling and Process Parameter
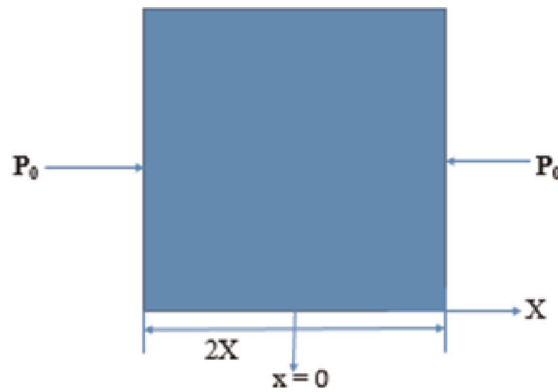
Figure 2.
Schematic representation of a square slab where P_o is microwave power flux (MW/m²) and 2X is the length of the slab.

2.2 Simulation parameter calculation process

Proximate analyses and ultimate analyses of coal were taken from Ref. [19]. Now, the amount of carbon monoxide required to convert hematite to magnetite was estimated by using equations given below (**Tables 1** and **2**) [21].

$$2\,C + O_2 = 2\,CO \tag{7}$$

$$\Delta G_f^0 = -111700 - 87.65T \tag{8}$$

$$3\,Fe_2O_3 + CO = 2\,Fe_3O_4 + CO_2 \tag{9}$$
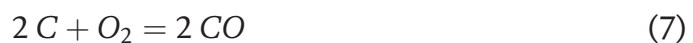
$$\Delta G_f^0 = -44300 - 39.89T \tag{10}$$

The fraction of coal needed is estimated using proximate and ultimate analyses, and we found that 7.5% of coal is required. Iron ore and coal powder were mixed

Parameter	Value (Wt. % dry basis)
Ash	9.89
Volatile	30.25
Fixed Carbon	59.86
Sulfur	1.03

Value calculated based on the data reported in Ref. [20].

Table 1.
*Proximate analyses of the coal sample.**

Parameter	Value (Wt.%, dry, Ash free)
Carbon	82.71
Hydrogen	5.39
Nitrogen	1.57
Sulfur	1.49
Oxygen	8.73

Value calculated based on the data reported in Ref. [20].

Table 2.
*Ultimate analyses of the coal sample.**

properly according to a stoichiometric calculation for the reduction of hematite into a desirable amount of magnetite.

Initial and final boundary conditions are given below:

$$t = 0 \ T = T0 \ 0 \leq x \leq X \tag{11}$$

$$x = 0 - k \frac{\partial T}{\partial x} = 0 \ t > 0 \tag{12}$$

$$-k \frac{\partial T}{\partial x} = h \left(T - T_\infty\right) + \varepsilon_\sigma \left(T^4 - T_\infty^4\right) \tag{13}$$

3. Results and discussion

The heating profile characteristic of hematite ore mixed with coal was modeled using simulation parameters of **Table 3**, **Figure 3** has demonstrated.

3.1 Temperature estimation

When solving the 1D heat equation, convection and radiation conditions were also considered. It is observed an increase in temperature till 100 s, and beyond this time, the increase in temperature is negligible. The temperature of the slab at the center (x = 0 m) is considered to be 30°C. After heating for 100 s, it gave an indication that the thermal runaway may occur during the microwave heating. Temperature profiles for different heating time periods 1s, 30 s, 60 s, 100 s, 200 s, 300 s, and 400 s (at 915 MHz

Parameter name	Value	Unit
K^*	$4.4072 - 32^*(10^{-4})\,^*T$	W/m/k
ρ	3866	kg/m^3
h^{**}	10	W/m^2°C
ϵ^{***}	0.96	None
T_0	25	°C
T_∞	25	°C
C_p^{****}	$211.122 - 0.10993^*T - 0.0003^*T^2\ 0.00000^*T^3$	J/kg/k
A	$K/(\rho * C_p)$	m^2/s
D_p (at 915HZ)*****	$0.4474 - 0.034 \times 10^{-3*}T + 2 \times 10^{-5}\,^*T^2 - 1 \times 10^{-7}\,^*T^3 - 6 \times 10{-}^{9*}T4 +$ $9 \times 10^{-13}\,^*T^5 - 4 \times 10^{-16}\,^*T^6$	mm

*Value calculated based on the data reported in Refs. [19, 22]
**Value calculated based on the data reported in Ref. [16].
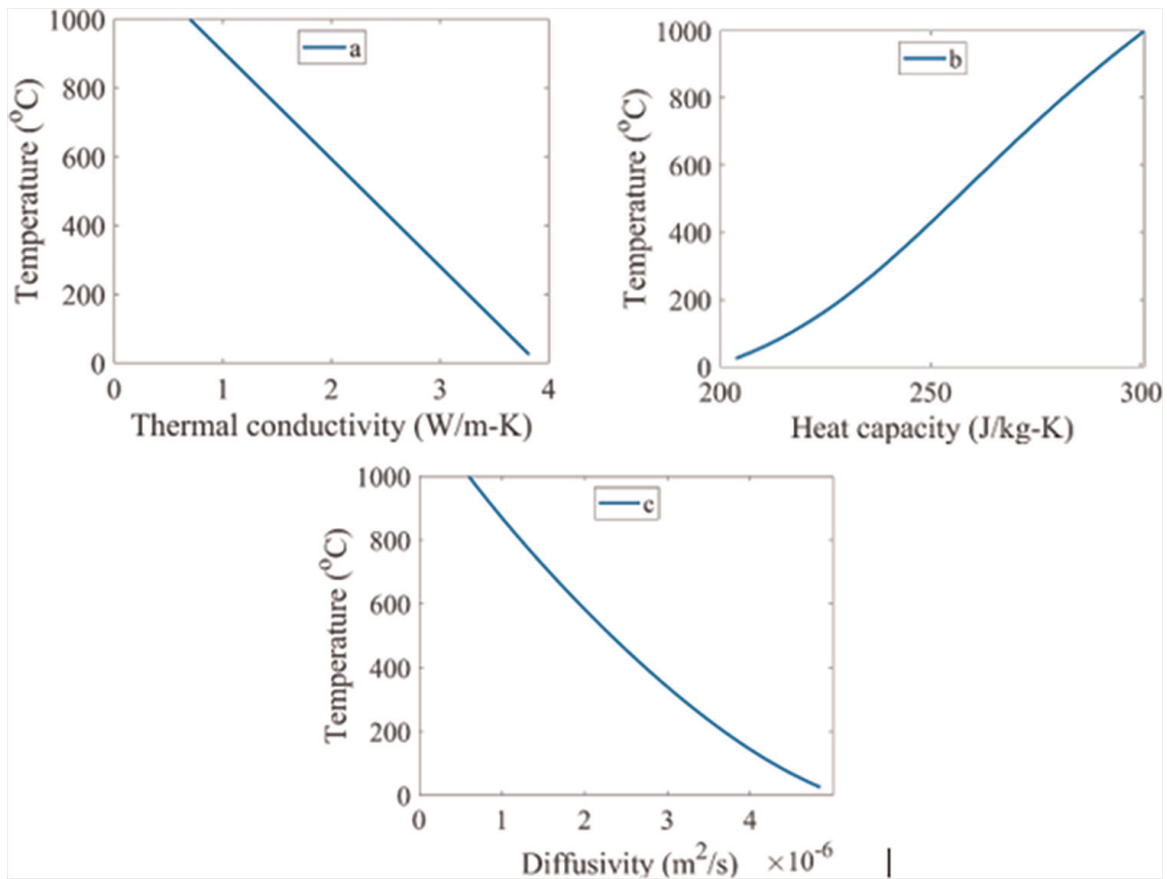****Value calculated based on the data reported in Ref. [19, 22].
***Value calculated based on the data reported in Ref. [16].
*****Value calculated based on the data reported in Ref. [19, 22–24].

Table 3.
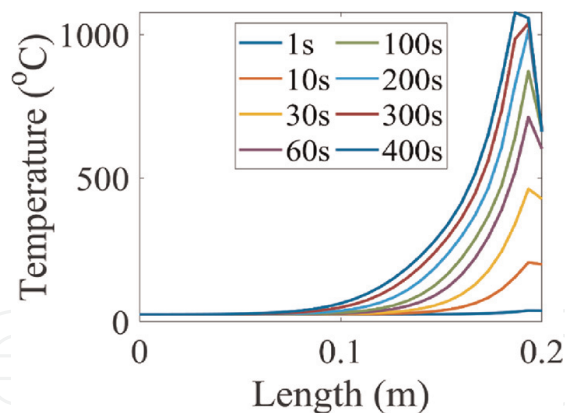*Thermophysical properties and modeling parameters were used in the simulation, and K, ρ, C_p, and D_p calculation process are shown in the Appendices.*

Figure 3.
*Temperature dependence on thermal conductivity, heat capacity, and thermal diffusivity.*

Figure 4
Temperature distribution in a 20 cm × 20 cm slab for different heating periods, viz., 1 s, 30 s, 60 s, 100 s, 200 s, 300 s, and 400 s, respectively, at a constant power.

and 1MW) are shown in **Figure 4**. The highest temperatures inside the object are around 33°C, 220°C, 415°C, 719°C, 912°C, 1016°C, and 1042°C for 1 s,10 s, 30 s, 60 s, 100 s, 200 s, 300 s, and 400 s respectively. Within the first 100 s of heating, the temperature in the 1D slab increases rapidly from 25 to 912°C. The reason for this rapid increase is due to the increase in thermal energy supplied by microwave radiation [8]. From 100 s to 400 s, the temperature increases from 912 to 1042°C. This increase is slower as compared to heating from 0 s to 100 s. It is mainly attributed to the initial heating (0–100 s). The thermal contribution from microwave heat generation dominates the temperature rise in the sample due to the weak thermal radiation effect due to the relatively low temperature of the object. As the heating continues, the temperature of the object increases, which leads to a high radiation effect. At higher temperatures, thermal conductivity reduces, and heat capacity increases. The heat diffusivity is found in **Figure 3c** to be in the order of 4×10^{-6} m^2 /s and decreases with increasing temperature. Heat capacity is found in **Figure 3b** to be 200 J/kg/K and increases with increasing temperature.

3.2 Temperature distribution across length for different powers of microwave

The 1D heat equation was solved by considering different values of power flux. Convection and radiation conditions were also considered. It was observed that there is an increase in temperature till a power flux of 2.5 MW/m^2, and beyond this power flux, the increase in temperature is negligible. Temperature profiles are plotted for a 1D slab with dimensions 0.20 m x 0.20 m. In this slab, different microwave powers (P_0) of 0.5, 1.5, 2.5, and 3.5 MW/m^2 were considered as shown in **Figure 5**. The temperature of the object increases with increasing microwave power. The highest temperatures attained in microwave heating for 60 s using different microwave powers of 0.5 MW/m^2, 1.5 MW/m^2, 2.5 MW/m^2, and 3.5 MW/m^2 are 370°C, 723.6°C, 1062°C, and 1112°C, respectively. Similarly, for times of 1 s, 120 s, and 180 s, temperatures attained are shown in **Table 4**. It is clear that if the source power increases, the microwave heating rate increases rapidly within 60 s. However, after 60 s, the temperature does not increase rapidly, even for higher microwave powers because of radiation and convection losses at high temperatures. It demonstrates that an appropriate power applied in microwave heating is influential in obtaining a high heating rate in a short time. On account of more radiation and convection heat losses to the
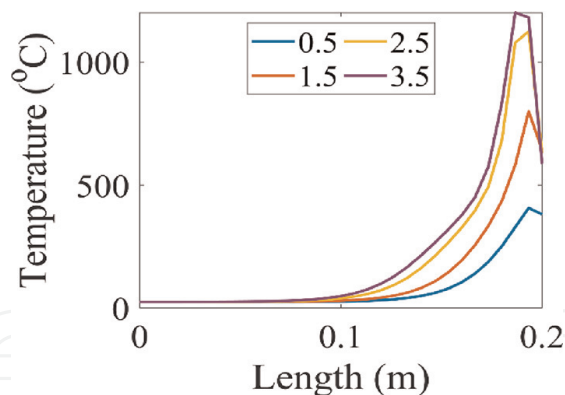
Figure 5.
Temperature distribution in a 20 cm × 20 cm slab by varying power flux, viz., 0.5 MW/m², 1.5 MW/m², 2.5 MW/m², and 3.5 MW/m², respectively, at a constant time of 50 s.

S.no.	Power flux (MW/m²)	Time (s)	Temperature (°C)
1	0.5	1, 60, 120, 180	27.8, 210.34, 441.63, 706.38
2	1.5	1, 60, 120, 180	30.58, 410.65, 757.98, 807.6
3	2.5	1, 60, 120, 180	39.67, 796, 850.4, 1025.6
4	3.5	1, 60, 120, 180	44.33, 1063.3, 1110.2, 1162.3

Table 4.
*Temperature distribution at various times and various power flux.*

environment at high temperatures, the peak migrates inward to keep heat balance between the object and surroundings.

3.3 Object Dimensions

Volumetric heating also depends on the object dimensions; it is shown in **Figure 6**. Temperature distribution in the slab with different dimensions of 0.01 m × 0.01 m, 0.05 m × 0.05 m, and 0.1 m × 0.1 m, respectively, were observed. More homogeneous temperature is achieved in samples of lesser dimensions than in larger dimensions. The highest temperature peak is obtained in a very short duration, which is an indication that more homogeneity was also observed. The temperature at the slab center increases from 25 to 84°C as the dimension decreases from 0.15 to 0.01 m. This indicates an optimal dimension of the material is required to obtain the minimum temperature nonuniformity and high heating performance. Here the highest temperature peaks for sample dimensions 0.01 m × 0.01 m, 0.05 m × 0.05 m, and 0.1 m × 0.1 m are 1000°C, 912°C, and 850°C, respectively.

3.4 Temperature distribution across length for different coal percentages

Microwave heating depends upon coal percentage in samples, as shown in **Figure** 7. The maximum peak temperature of the slab with different coal percentages (6.5%, 7.5%, and 8.5%) is 736°C, 743°C, and 753°C, respectively were found. Coal, a carbonaceous material, absorbs microwave energy, resulting in an increase in temperature. Guang Xu et al. [23, 24] reported that coal could enhance permeability, loss factor, and
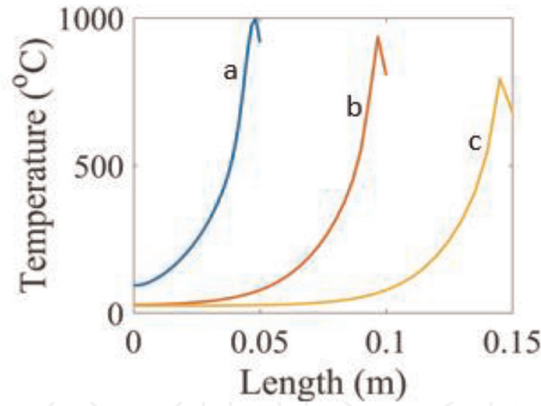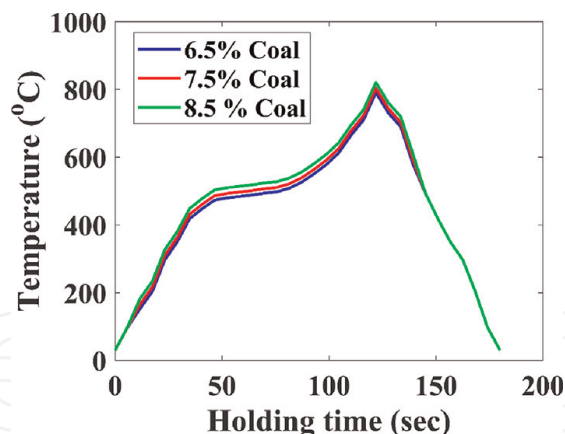
Figure 6.
Temperature distribution in the hematite slab of dimensions, 0.01 m × 0.01 m (a), 0.05 m × 0.05 m (b), and 0.1 m × 0.1 m (c) for a constant heating period of 60 s and power of 1 MW/m².
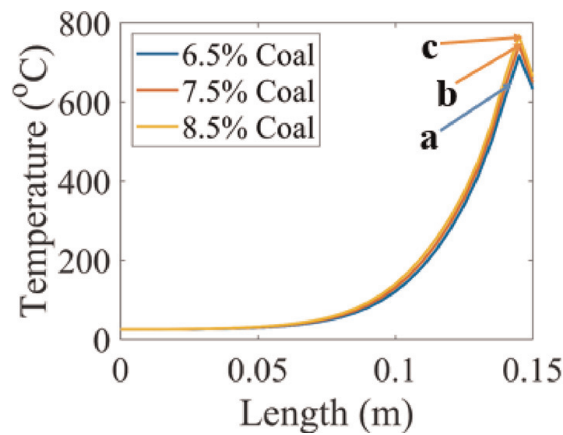
Figure 7.
Temperature distribution in the hematite slab of dimensions, 0.15 m × 0.15 m and coal percentage (a), 6.5 (b), 7.5, and (c) 8.5 for a constant heating period of 180 s and power of 1 MW/m².

dielectric constant of mixture samples and ensure the optimal heating effect. D_p (depth of penetration) of microwave heating is directly proportional to $\sqrt{\frac{\varepsilon''}{\varepsilon'}}$, The loss tangent is defined as $\tan\delta = \frac{\varepsilon'}{\varepsilon''}$. The attenuation constant, $\alpha = \frac{2\pi}{\lambda}\left[\frac{\varepsilon'}{2}\left(\sqrt{1+(\tan\delta)^2}-1\right)\right]^{1/2}$ represents the rate of absorption of the wave into the sample. Finally, the output of penetration depth is achieved by $D_p = \frac{1}{2\alpha}$, so the depth of penetration is inversely related to the attenuation. So, it can say coal increases the loss factor and the dielectric constant of the samples increases. For that, penetration depth will be enhanced of the samples, which also respond to temperature increases. The temperature peak (**Figure 7**) is seen at similar locations in all three samples because the D_p expression accounts for the loss factor and permeability also. During microwave heating for lean iron ore (Fe – 58%, Si – 42%, MNDC, Hyderabad) beneficial (Fe_2O_3 to Fe_3O_4) purposes coal percentage should be limited (7.5%) when coal composition as per **Table 2**. Otherwise, the temperature will increase, and a non-magnetic phase (FeO) will be produced. Because above 800°C temperature formation of FeO and Fe is dominant due to the high rate of carbon gasification. Therefore, more than 7.5% carbon is not a desirable carbon percentage for the reduction study in the microwave furnace for such type of lean iron ores

9

Figure 8.
Variations of temperature with blowing time-varying carbon 6.5%, 7.5%, and 8.5%, respectively.

3.5 Verification with experiment results

Temperature variations of the samples for 6.5, 7.5, and 8.5 coal is shown in **Figure 8**. Our model predictions are consistent with experimental results, which found temperature increases from 791°C to 821° C when coal content in the samples increases from 6.5% to 8.5%.

3.6 Sample preparation

Received iron ore is pulverized in a ball mill for 30 min with 10 mm diameter steel balls. The milled powder is further sieved to below 100 μm (-100 mesh size). The composition of iron ore samples is (65 % Fe_2O_3 and 35% SiO_2). The proximate analysis result of coal is given below in **Table 1**. 100 grams of iron ore and the stoichiometric amount of reducing agent like 7.5 gram coal are entirely mixed. Then, using this mixture, pellets are made with dimensions of 15 mm × 15 mm by pressing the machine. (5 T pressing m/c, VB Ceramic). The pressing condition is 2-ton load and dwells time, 2 min. Each pellet weight varies about 6 gm. Three samples were made by changing carbon percentages to 6.5, 7.5, and 8.5.

3.7 Microwave treatment

A power (1 MW) and 2.45 GHz hybrid microwave oven (VB Ceramic, Chennai, India) was used for microwave heating. Samples were placed in the oven in a microwave in an alumina crucible. The crucible was located in the central position of the microwave chamber to minimize the effect of the field pattern variations in the oven. Then heating is performed at 800°C for 3 minutes.

4. Conclusions

In this study, microwave heating effects were discussed in detail, which can be very useful in verifying the microwave-assisted carbothermal reduction process of hematite slab in iron-making plants. Even though the findings are valuable in optimizing microwave heating parameters for reduction, further verification is needed before implementing them in plants. Numerical simulations of heat transfer in one-

dimensional hematite 20 cm x 20 cm slab under microwave irradiation by considering conduction, convection, and radiation effect, concludes the following

1. The temperature distribution inside the object is nonuniform.

2. The temperature in the object increases rapidly from 0 s to 100 s due to the quick transfer ofthermal energy to the object by microwave irradiation. However, after 100 s of heating, the temperature does not increase rapidly due to higher thermal radiation and convection losses.

3. A pre-determined microwave power source is required to attain the highest temperature of the hematite slab within 100 s.

4. Highest peak temperature of the slab increased from 736°C to 753°C using model prediction and 791°C to 821°C using experiments respectively due to increased coal percentage from 6.5% to 8.5%.

Acknowledgements

Conflicts of interest

The authors declare no conflict of interests.

Nomenclatures

P_0 Microwave power flux (MW/m^2)
T   Temperature (°C)
ρ Density (Kg/m^3)
c_p Specific heat (J/kg-K)
k   Thermal conductivity (W/m-K)
D_p Depth of penetration (m)
t   time (s)
T_0 Initial temperature (°C)
T_∞ Environmental temperature (°C)
h   Heat transfer coefficient (W/m^{2}k)
ε Emissivity (W/m^2)
σ Stefan-Boltzmann constant (W·m^{-2}.K^{-4})
μ_r' The real part of permeability (-)
μ_r'' The complex part of permeability (-)
X   Half-length of slab (m)
ε_r' The real part of permittivity
ε_r'' The complex part of permittivity (-)
ε' dielectric constant (-)
ε'' loss factor (-)

A. Appendices

Density, permittivity, and permeability, specific heat calculation process after mixed

The density of mixture = $\dfrac{M_t}{\dfrac{M_a}{\rho_a} + \dfrac{M_b}{\rho_b}}$

M_t = total mass of mixture

M_a = mass of component a

ρ_a = density of component a

M_b = mass of component b

ρ_b = density of component b

$\ln \varepsilon = V_{iron}\, \varepsilon_{iron} + V_{coal}\, \ln\varepsilon_{coal}$

V_{iron} = Volume fraction of iron ore

V_{coal} = Volume fraction of coal

$\ln\varepsilon' = V_{iron}\, \varepsilon'_{iron} + V_{coal}\, \ln\varepsilon'_{coal}$

$\ln\varepsilon'' = V_{iron}\, \varepsilon'_{iron} + V_{coal}\, \ln\varepsilon'_{coal}$

V_{iron} = volume fraction of iron ore

V_{coal} = volume fraction of coal

C_p of mixture = $\dfrac{M_a}{M_{mix}} C_{p_a} + \dfrac{M_b}{M_{mix}} C_{p_b}$

M_a = mass of component a

M_b = mass of component b

M_{mix} = total mass of components a and b

C_{p_a} = Specific heat of component a

C_{p_b} = Specific heat of component b

Author details

Prasenjit Singha[1*], Sunil Yadav[1†], Soumya Ranjan Mohanty[1†], Abhishek Tiwari[2] and Ajay Kumar Shukla[1]

1 Department of Metallurgical and Materials Engineering, IIT Madras, Chennai, Tamil Nadu, India

2 Department of Metallurgical and Materials Engineering, Indian Institute of Technology Kharagpur, West Bengal, India

*Address all correspondence to: psinghanifft@gmail.com

† These authors contributed equally.

IntechOpen

References

[1] Kusuma J, Ribal A, Mahie AG. International Journalof Differential Equations and Applications. 2018, 2018;**2018**:1

[2] Yoshikawa N, Ishizuka E, Ashiko KM, Chen Y, Taniguchi S. ISIJ International. 2007;**47**:523

[3] Malmberg D, Hahlin P, Nilsson E. ISIJ International. 2007;**47**:533

[4] Makino Y. ISIJ International. 2007;**47**:539

[5] Peng Z. Michigan Technological University, Michigan

[6] Vadivambal R, Jayas DS. Journal of Food and Nutrition Research. 2010;**3**:161

[7] Hayashi M, Takeda K, Kashimura K, Watanabe T, Nagata K. ISIJ International. 2013;**53**:1125

[8] Barani K, Javad Koleini SM, Rezaei B. Separation and Purification Technology. 2011;**76**:331

[9] Standish N, Huang W. ISIJ International. 1991;**31**:241

[10] Agrawal S, Dhawan N. Metal Material Transaction B. 2020;**51**:1576

[11] Mishra S, Roy GG. Metallurgical and Materials Transactions B. 2016;**47**:2347

[12] Zhulin L, Xuegong B, Zeping G, Wei L. Advanced Materials Science and Engineering. 2018;**2018**:1

[13] Nishioka K, Taniguchi T, Ueki Y, Ohno K, Maeda T, Shimizu M. ISIJ International. 2007;**47**:602

[14] Mishra P, Upadhyaya A, Sethi G. Metals, Metallurgical and Materials Transactions B: Process Metallurgy and Materials Processing Science. 2006;**37**:839

[15] Shukla AK, Mondal A, Upadyaya A. Science of Sintering. 2010;**42**:169

[16] Peng Z, Hwang JY, Mouris J, Hutcheon R, Huang X. ISIJ International. 2010;**50**:1590

[17] Zhiwei P, Hwang J-Y, Andriese M, Bell W, Huang X, Wang X. ISIJ International. 2011;**51**:884

[18] Peng Z, Yang Hwang J, Gon Kim B, Mouris J, Hutcheon R. Energy & Fuels. 2012;**26**:178

[19] Peng Z, Hwang JY, Mouris J, Hutcheon R, Sun X. Metals, Metallurgical and Materials Transactions. 2011;**42**:2259

[20] Molgaard J, Seltzer WW. Journal of Applied Physics. 2003;**42**:3644

[21] Ghosh A, Chatterjee A. Ironmaking and Steelmaking Theory and Practice. New Delhi: PHI Learning Private Limited; 2012. pp. 55-87

[22] Hu W, Deng J, Li Q-W, Yang X, Shu C-M, Zhang Y-N. Thermochemical Acta. 2017;**656**:101

[23] Leão TP, Perfect E, Tyner JS. Transactions of the ASABE. 2015;**58**:83

[24] Xu G, Huang J, Hu G, Yang N, Zhu J, Chang P. Fuel Processing Technology. 2020;**202**:1